

Article

Contribution of TEMPO-Oxidized Cellulose Gel in the Formation of Flower-Like Zinc Oxide Superstructures: Characterization of the TOCgel/ZnO Composite Films

Khalil Jradi *, Chloé Maury and Claude Daneault

Lignocellulosic Materials Research Center, University of Quebec at Trois-Rivières, des Forges avenue 3351, 500 Trois-Rivières, QC G9A-5H7, Canada; E-Mails: chloe.maury@uqtr.ca (C.M.); claude.daneault@uqtr.ca (C.D.)

* Author to whom correspondence should be addressed; E-Mail: khalil.jradi@uqtr.ca or khalil.jradik@gmail.com; Tel.: +1-819-376-5011; Fax: +1-819-376-5148.

Academic Editor: Raed Abu-Reziq

Received: 15 October 2015 / Accepted: 3 November 2015 / Published: 13 November 2015

Abstract: In the present paper, we report on a simple and new approach for the synthesis of hierarchical flower-like zinc oxide superstructures ZnO (FL) in the presence of the TEMPO-oxidized cellulose gel (TOCgel) through a room temperature sol-gel process in aqueous medium. Resulting composite films based on TOCgel and ZnO were investigated by several techniques including scanning electron microscopy (SEM), Fourier transform infrared spectroscopy (FTIR), X-ray photoelectron spectroscopy (XPS), thermogravimetric analysis (TGA) and mechanical tests. SEM images demonstrated the formation of well-shaped flower-like ZnO superstructures within the fibrous structure of the TOCgel with a uniform diameter (~5 μm). FTIR and XPS results clearly confirmed the formation of such ZnO structures. We suggested that the carboxylate groups of TOCgel fibers act as capping agents and promote the construction of such flower-like ZnO via a nucleation-growth process. A proposed mechanism based on the oriented attachment-driven growth was discussed in order to explain the formation of ZnO (FL). The photocatalytic activity of the TOCgel/ZnO composite in the degradation of methylene blue (MB) under UV irradiation was clearly confirmed. Finally, mechanical tests demonstrated that the former TOCgel/ZnO film maintained a good flexibility (bent up to ~120°) without losing its photocatalytic activity.

Keywords: TEMPO-oxidized cellulose gel; flower-like ZnO; crystal growth; sol-gel; composite

1. Introduction

In recent years, the controlled synthesis of inorganic particles and their morphologies are of strong interests due to the fact they have very important potential as optical, sensor, catalytic, and electrical materials [1–4]. Among those, zinc oxide ZnO has been used as a useful candidate for various applications due to their unique optical and electrical properties, which renders it suitable in many application fields from optoelectronics to energy conversion, hydrophobic and electrowettable surfaces, piezoelectric, nanogenerators, gas sensing, and photocatalytic systems [5–12].

It is well known that the physical properties of ZnO are strongly dependent on its morphology and size [13]. Numerous researchers have paid considerable attention to the micro/nano-structures systems, especially three-dimensional hierarchical superstructures that are assembled by nanoscale building blocks such as nanoplates, nanowires, nanosheets and nanorods [14,15].

Therefore, considerable efforts have been devoted to design of effective methods to synthesize ZnO with tunable size and morphology. Over the past decades, various methods have been developed to synthesize ZnO with various morphologies such as physical and chemical vapor deposition, thermal evaporation, metal-organic chemical vapor deposition and wetting chemical synthesis, template-assisted growth and solution-based approaches [16–18]. During the last decades, various studies concerning the control of the nucleation and the growth of ZnO nano/microstructures embedded in polymeric matrices have been reported, with a special emphasis on the particles morphological control and its influence on their physical properties [19,20]. In this context, Chiolerio *et al.* have developed a method to fabricate a mem-sensor in which ZnO wires embedded in a polymeric matrix are ordered to create morphological anisotropy by means of dielectrophoresis [21].

For these reasons, several works were performed in order to tune the shape and the size of ZnO structures using different capping agents capable of stabilizing a particular crystal facet by adsorption and alter the growth rate in different crystal planes [22,23]. Moreover, different soft templates/capping agents such as water-soluble polymers [24–26], citrate salts [27,28], surfactants [29–31], a mixture of sodium citrate and alkylamine [23], citric acid [25], ethylene diamine [32], and amino acids [33] have been successfully used in wet-chemical methods. In this context, Sun *et al.* have developed a method to fabricate novel flower-like 3D ZnO superstructures in aqueous solution and using trisodium citrate dihydrate as a surfactant to enhance the nucleation-growth process implied in the formation of such hierarchical superstructures [34]. Multilayered ZnO nanosheets with porous structures were synthesized by simple calcination of the hydroxide zinc carbonate at 400 °C in air ambient to be used as acetone sensors [35].

Gazia *et al.* have developed a simple method to fabricate a coral-shaped porous ZnO nanostructure by room temperature sputtering processes [36]. Ko *et al.* also reported the formation of novel ZnO hierarchical nanowires for high efficiency dye-sensitized solar cells [37]. Moreover, using a solvothermal approach in an aqueous solution of ethylene diamine, Lu *et al.* prepared ZnO hierarchical micro/nanostructures possessing enhanced photocatalytic performance [38]. Prism-like and flower-like ZnO structures with good photocatalytic activities were synthesized through a hydrothermal route in the presence of amino acid [39]. Yin *et al.* also developed novel ZnO nanorod-assembled hollow superstructures for photoluminescence and catalysis applications using hydrothermal reaction via sodium carboxymethyl cellulose (CMC) assistance [40]. Flower-like ZnO nanostructures with controllable sizes

and higher catalytic activity were fabricated through a solution-phase route in the presence of ascorbate as a shape directing/capping agent [41].

However, these above-mentioned methods require high temperature and introduce impurities in the final products when templates and catalysts are used in the reaction system. Moreover, most organic additives used in these methods were expensive long chain molecules.

Recently, ZnO particles attached onto biopolymers have been the subject of increasing interest in the field of composite materials [42,43]. Among them, cellulose and their derivatives were chosen as good candidates for enhancing the physical properties of the ZnO/cellulose composite. Furthermore, using cellulose-based materials is practical because cellulose is the most abundant polymer found in nature, inexpensive, easy to process, renewable, biodegradable, and biocompatible [44]. There are several works on the literature concerning the incorporation of ZnO particles in cellulose and its derivatives [45,46]; however, studies in which oxidized nanocellulose has been used as a capping agent to control the morphology of ZnO particles has never been reported. In our study, a flexible TEMPO-oxidized cellulose gel (TOCgel)/ZnO composite film was synthesized through a hydrothermal sol-gel process at room temperature. In this work, nanocellulose gel was obtained through 2,2,6,6-tetramethylpiperidinyl-1-oxyl (TEMPO)-mediated oxidation, which is one of the regioselective chemical modifications of primary hydroxyl groups located on the cellulose fibers [47]. The advantage in using TOCgel as a reinforcement agent in the composite film is because TOCgel, considered as a cellulosic nanomaterial (5–20 nm wide single-sized microfibrils), is composed of crystalline and amorphous domains that are generated by the TEMPO-oxidation process [48]. At the same time, carboxyl (COOH) and hydroxyl (OH) moieties mostly present in the amorphous domain make TOCgel highly reactive and consequently, improve the interaction forces (electrostatic, Van der Waals, hydrogen bonding) with Zn^{2+} and ZnO species and, consequently, promote the formation of hierarchical flower-like ZnO superstructures during the sol-gel synthesis, which will be discussed in detail later in this study.

In this paper, we describe a simple approach for the synthesis of a flexible composite film based on TEMPO-oxidized cellulose gel and zinc oxide particles through a hydrothermal route. Herein, polar moieties of TOCgel (especially carboxyl groups) play an important role in the driving growth mechanism of the formation of ZnO superstructures onto cellulose fibers surfaces and precisely on nucleation-growth processes. Finally, the former TOCgel/ZnO (FL) composite film was characterized by different techniques, and its photocatalytic activity in the degradation of methylene blue (MB) was also performed. A proposed mechanism explaining the formation of ZnO superstructures directly grown onto the oxidized nanocellulose backbone was discussed.

2. Experimental Section

2.1. Materials

Zinc nitrate hexahydrate ($Zn(NO_3)_2 \cdot 6H_2O$), hexamethylenetetramine HMT ($C_6H_{12}N_4$, 99% purity), sodium bromide (NaBr), sodium hypochlorite (NaOCl), 4-acetamido-TEMPO (2,2,6,6-tetramethylpiperidin-1-oxyl) and methylene blue ($C_{16}H_{18}ClN_3S \cdot 3H_2O$) were purchased from Sigma Aldrich (St Louis, MO, USA) and used as received. A commercial never-dried bleached Kraft hardwood pulp was used as the cellulose sample for the production of TOCgel through the TEMPO-mediated

oxidation and mechanical treatments. Analytical grade chemicals and solvents were always used as received without further purification.

2.2. Methods

2.2.1. Production of TEMPO-Oxidized Cellulose Gel (TOCgel)

In the first step, the oxidation of native cellulose fibers was carried out by the TEMPO-mediated oxidation system [49] and conducted in a 45L flow-through sonoreactor (semi-continuous mode) with a nominal input power capacity of 2000W (262 W/L, 12300 W/m²), according to the procedure developed in our laboratory [47,50]. The experimental process based on TEMPO-mediated oxidation used in the preparation of TOCgel was illustrated in Figure 1.

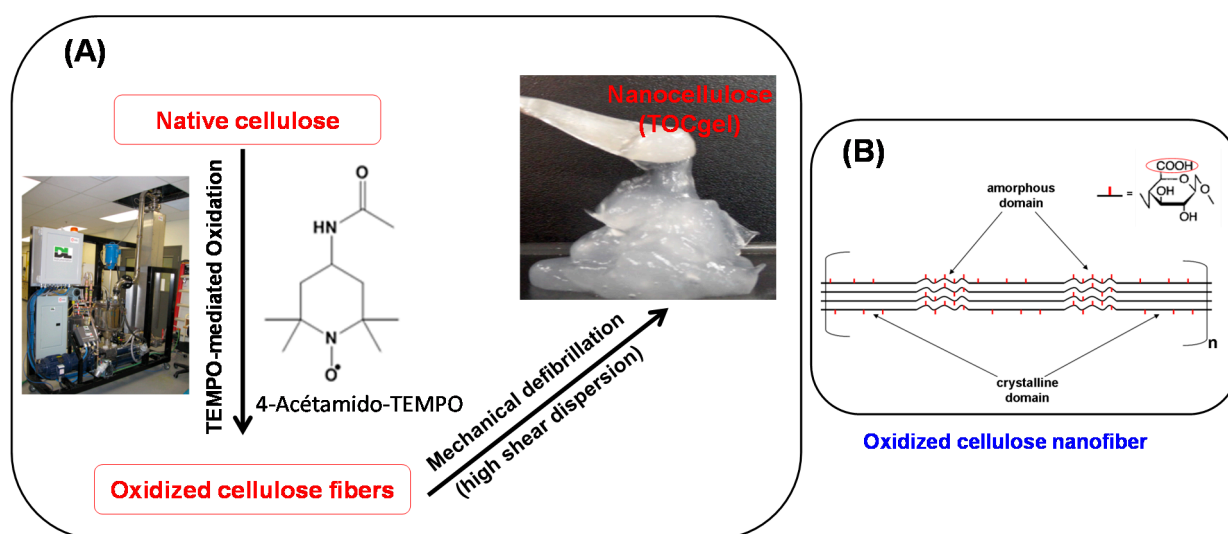


Figure 1. Schematic representation of the experimental process used in the production of oxidized cellulose gel (A); and the TEMPO-oxidized cellulose nanofiber (B).

Before oxidation, 400 g of dried bleached hardwood pulp were pre-soaked for an overnight in 40 L of deionized water at room temperature. The soaked pulp was disintegrated for 5 min in a laboratory disintegrator to obtain a uniform fiber suspension of about 1% consistency. To the cellulose suspension, we added 9.2 g of 4-acetamido-TEMPO and 25 g of sodium bromide. A solution of NaOCl (3.1 mmol/g) was added dropwise to the mixture at room temperature under gentle agitation during the first 30 min. The pH was maintained at 10.5 by adding 0.5 M NaOH. After the pH was stabilized, the reaction was stopped after 90 min by adding 1 L of H₂O₂ (1%). The TEMPO-oxidized product was filtered, washed thoroughly with deionized water, and stored at 4 °C. Then, the carboxylate content of the oxidized cellulose was determined using an electrical conductivity titration method [49], and it was equal to ~1.2 mmol/g. The obtained carboxylate celluloses were used to make the oxidized cellulose gel. In the second step, TEMPO-oxidized cellulose gel (TOCgel) was prepared by high shear dispersion of oxidized pulp in a wet colloid milling apparatus (MK 2000/4) from IKA Works, Inc. (Cincinnati, OH, USA). Briefly, the oxidized pulp suspension (2 L) was pumped from an agitated tank between a conical rotor and a stator in the MK mill in closed loop for one hour to obtain TOCgel material (3% consistency) [47]. Then,

carboxylate groups created on the cellulose microfibrils by the TEMPO-mediated oxidation have anionic charges in water. These charges induce electrostatic repulsions between the microfibrils, which consequently help the defibrillation process and contribute to the formation of individual microfibrils [51].

2.2.2. Synthesis of ZnO Powder and TOCgel/ZnO Composite Films

In our experiment, a sol-gel process was used in the preparation of ZnO particles and TOCgel/ZnO composite films in aqueous medium at room temperature.

TOCgel/ZnO Composite Film Preparation

TOCgel/ZnO composite films was prepared by initially dispersing 0.25 g of TOCgel in water (50 mL). To this suspension, 30 mL of Zn (NO₃), 6H₂O (0.1 M) was added and allowed to react for 30 min. Then, 30 mL of HMT (0.1 M) was added dropwise to the mixture and allowed to react for one hour in the ambient air under gentle agitation. The resulting structure was then collected on a filter paper in a Buchner funnel using reduced pressure and thoroughly washed with ethanol and deionized water. The filter paper was subsequently removed and the TOCgel/ZnO composite film was air-dried in the clean oven at 70 °C for an overnight. Different concentrations of zinc nitrate (ranging from 5 to 40 mM) were used to study their effect on the morphological state of ZnO structures incorporated into the former composite film.

Pure ZnO Preparation

Pure ZnO powder was synthesized by mixing 30 mL of Zn (NO₃); 6H₂O (0.1 M) with 30 mL of HMT (0.1 M) under the sol-gel process at room temperature. The reaction proceeded for one hour, after which, the white solid residue was collected on a filter paper within a Buchner funnel using reduced pressure and then thoroughly washed with ethanol and water, and air-dried in the clean oven at 70 °C for an overnight.

2.3. Characterization

The SEM images of typical samples were obtained with a JEOL JSM-5500 Scanning Electron Microscope (JEOL, Kyoto, Japan). Samples were gold coated using an Instrumental Scientific Instrument PS-2 coating unit. The SEM operating voltage was at 15.0 kV.

FTIR spectra of samples were performed at 16 scans and a 4 cm⁻¹ resolution in transmission mode with a PerkinElmer 2000 Fourier transform infrared spectrometer (Buckinghamshire, UK). The samples were mixed with potassium bromide (KBr) and the scan range was fixed in the region between 400 and 4000 cm⁻¹.

Thermal stability analysis (TG/DTG) of samples was carried out in a Perkin-Elmer thermoanalyzer (Yokohama, Kyoto, Japan). Samples of pure TOCgel and composites were heated in open platinum pans from 50 to 600 °C, under a nitrogen atmosphere, at a heating rate of 5 °C/min. Then, samples were heated from 600 to 1000 °C under air at a heating rate of 10 °C/min.

XPS measurements were performed with a Kratos Ultra electron spectrometer (AXIS ULTRA, Kratos, Manchester, UK, 2000) using a monochromatic (AlK α) X-ray source ($k = 1486.6$ eV) with a power of 225 W, at a take-off angle of 90° relative to the sample surface. The low-resolution survey scans were taken with a 1 eV step and 160 eV analyzer pass energy. High-resolution spectra were taken

with a 0.1 eV step and 40 eV analyzer pass energy. The analysis area was less than 1 mm² and measurements were taken at two different locations on each of the touching faces of pure TOCgel and TOCgel/ZnO composite film. The collected data were analyzed using Vision software version 2.1.3 and CASA XPS version 2.3.15 (Kratos, Manchester, UK, 2013).

Tensile Tests of pure TOCgel and TOCgel/ZnO composite films were performed on a universal testing machine (INSTRON 4201, Instron, Canton, MA, USA) at room temperature with a gauge length of 10 mm and cross-head speed of 10 mm/min. The average value of five replicates for each sample was taken.

Finally, the photocatalytic activity of the pure ZnO and TOCgel/ZnO composite films in the degradation of MB (10 mM) was performed in air at ambient temperature. The same amount of each sample (50 mg) was immersed in 50 mL of MB solution and then exposed to ultra-violet irradiation from a 15W Hg lamp (model UVL-56, UVP, Upland, CA, USA) for 2 h. After that, the absorbance of MB was measured using a UV-vis spectrometer (Cary 5000 spectrophotometer, Varian, Melbourne, Australia). The photocatalytic efficiency was evaluated in terms of the decrease of the absorption peak intensity of MB at 665 nm which indicates the degradation of the MB during the UV-irradiation.

3. Results and Discussion

The main goal of this work was to investigate the contribution of TOCgel (up to 80% nanofibers) in the crystal growth of hierarchical flower-like ZnO superstructures through a hydrothermal synthesis at room temperature. In this study, hexamethylenetetramine (HMT) was used as a catalyst and a source of base (*i.e.*, OH⁻) in precipitation and formation processes of ZnO particles during the reaction medium. Thus, the obtained composite films based on TOCgel and ZnO were analyzed by different techniques in order to confirm the formation of ZnO superstructures onto the cellulose fibers surfaces and to investigate their mechanical and photocatalytic properties. A mechanism explaining the formation of ZnO superstructures was discussed in detail later in this section.

3.1. SEM Analysis of TOCgel/ZnO Composites' Characterization

Figure 2 exhibits typical scanning electron microscopy (SEM) images of TOCgel/ZnO composite films prepared with different concentrations of zinc nitrate hexahydrate in the presence of HMT through the hydrothermal route at room temperature. In the present work, the contribution of carboxylate moieties of TOCgel in the tuning of the shape of ZnO structures directly grown within the cellulosic fibrous structure was studied. In comparison with the pure TOCgel (Figure 2A), our results indicate that the amount and the morphology of well-dispersed ZnO clearly depend on the concentration of Zn²⁺ introduced in the reaction.

A low-magnification view of composite films shown in Figure 2B–E demonstrates the formation of uniform flower-like ZnO superstructures well-dispersed onto TOCgel surfaces and having an average diameter of about 5 μm. However, when the concentration of Zn²⁺ is too low (50 mM), the flower-like ZnO structure appears to be not completely achieved (Figure 2B). The increase of the Zn²⁺ concentration (≥10 mM) strongly enhances the formation of a large quantity of well-shaped flower-like ZnO superstructures within the fibrous 3D network of TOCgel (Figure 2C,D). In addition, the size of these ZnO superstructures remains unchanged and is equal to 5 μm approximately. The dimension of these

superstructures was in agreement with the work of Wang *et al.*, which synthesize flower-like ZnO superstructures with approximately 5 μm diameter [52].

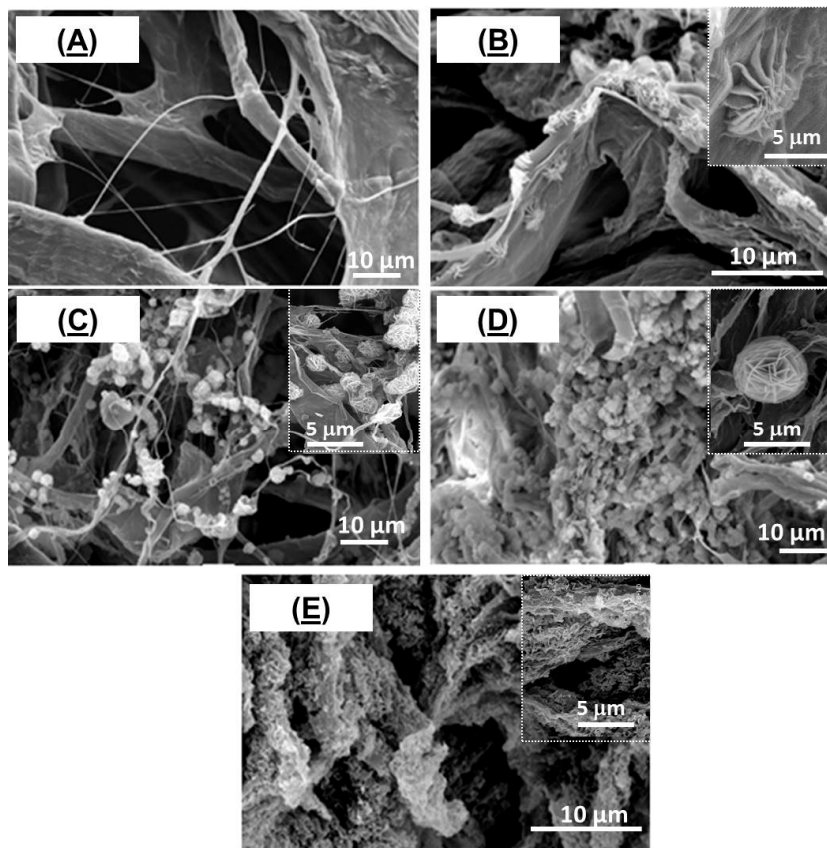


Figure 2. SEM images of TOCgel/ZnO composite films prepared with different concentrations of Zn^{2+} : 0 mM (A); 5 mM (B); 10 mM (C); 20 mM (D) and 40 mM (E).

Moreover, higher concentration of Zn^{2+} (≥ 40 mM) leads to higher amount of ZnO superstructures which appear more collapsed and denser as shown in Figure 2E. In this case, the surface of cellulose fibers is covered by a continuous and relatively homogeneous-deposited ZnO coating. However, the resulting thick coating ZnO render the final composite film brittle and could not be suitable due to its poor mechanical behavior (very brittle). Furthermore, to study the effect of carboxylate groups (COO^-) of TOCgel (~ 1.2 mmol/g) on the morphology of ZnO architectures, we prepared a composite film based on native cellulose fibers (~ 0.05 mmol/g) and ZnO under reaction conditions similar to that used for the TOCgel/ZnO composite film. Interestingly, we did not observe any regular flowerlike morphology via SEM (Figure 3A) of this sample (lower carboxylate amount); rather, some aggregated structures with undefined morphologies were observed.

In comparison with SEM images provided in Figures 2 and 3, it is evident that the flower-like ZnO superstructures are formed only in the presence of carboxylates, which indicate the crucial role of carboxylate moieties of TOCgel in nucleation and growth process of ZnO in a particular direction that ultimately results in the formation of such anisotropic flower-like morphology, which is in accordance with the results reported elsewhere by other researchers [41]. These results indicate that the flower-like ZnO architectures can be formed in the presence of ascorbate ions which are similar to carboxylate moieties of oxidized cellulose material (TOCgel). In addition, the presence of carboxylate functions onto

cellulose fibers surfaces enhances the individualization state of cellulose nanofibers and consequently, facilitates the diffusion phenomena of chemical reactants (*i.e.*, Zn^{2+} ; HMT, OH^-) in the cellulosic material. Consequently, this phenomenon leads to the formation of well-dispersed ZnO superstructures onto the TOCgel network. Moreover, we prepared pure ZnO using the same hydrothermal conditions in the presence of HMT and without the addition of cellulose fibers in the reaction medium.

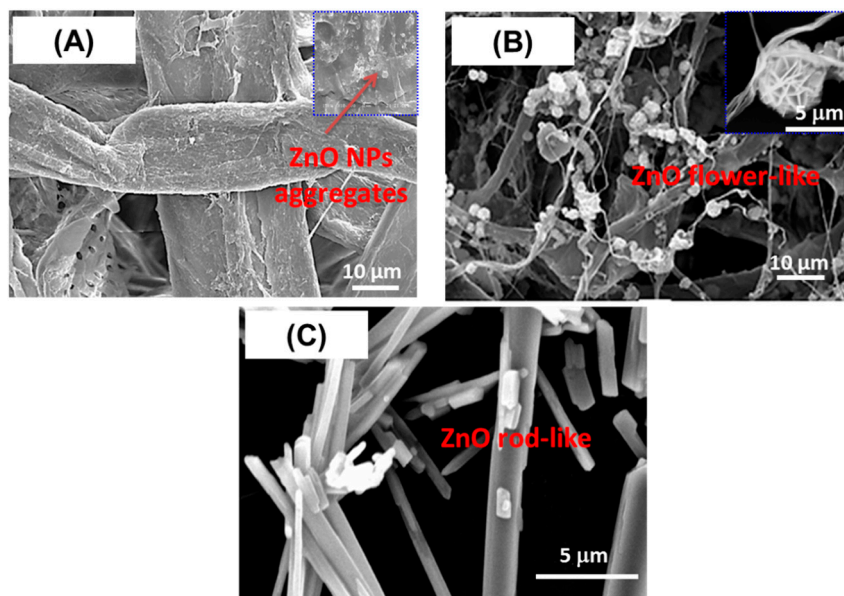


Figure 3. SEM images of samples films synthesized with two types of cellulose fibers: (A) native cellulose fibers; and (B) oxidized cellulose (TOCgel); and without cellulose (C).

In comparison with the heterogeneous nucleation observed in the presence of cellulosic fibers, SEM images demonstrated the formation of rod-like ZnO microstructures which could be obtained through the homogeneous nucleation directly in the solution (Figure 3C). According to the literature [53], the adsorption of HMT chains onto the non-polar facets of zincite crystal (*i.e.*, 100, 110 and 010) promotes the epitaxial growth of ZnO along the *c*-axis and leads to the formation of rod-like ZnO microstructures as shown in Figure 3C. In addition, an alignment phenomenon of flower-like ZnO superstructures has been observed in the TOCgel/ZnO composite film.

This is further supported by high magnification SEM, which demonstrated the alignment state of ZnO superstructures along the main cellulosic fibers axis (Figure 4). In fact, the physical interaction (*i.e.*, hydrogen bonding, electrostatic and van der Waals forces) between polar moieties (carboxylate and hydroxyl) of TOCgel on the one hand, and polar species of ZnO crystal (basal plane 001) and Zn^{2+} ions on the other hand could explain the incorporation state of ZnO superstructures along the cellulose fiber axis.

As shown in Figure 4, the alignment of flower-like ZnO superstructures towards the composite film is well-characterized by a 5 μm width, which is similar to the diameter of a single flower-like ZnO structure observed in this composite. This indicates that the former TOCgel/ZnO (flower-like) possess specific anisotropic microstructures.

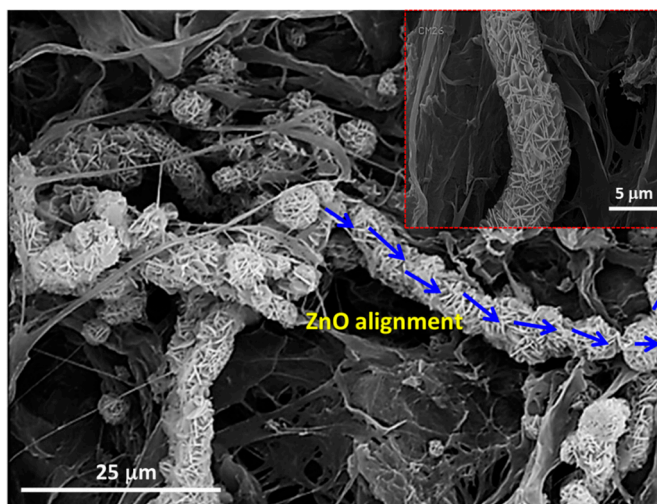


Figure 4. SEM images of TOCgel/ZnO composite film indicating the alignment of flower-like ZnO superstructures.

In order to explain the growth mechanism involved in the formation of these superstructures, a physical and chemical approach will be discussed in detail later in this section.

3.3. FTIR and XPS Results

Figure 5 showed the FTIR spectra of pure ZnO, pure TOCgel and TOCgel/ZnO composite films. FTIR spectrum of the pure ZnO showed a high intensity broad band around 480 cm^{-1} due to the stretching mode of the zinc and oxygen bond [54]. The similar band was also observed in the case of TOCgel/ZnO confirming the presence of ZnO species in the final composite. In addition, FTIR spectrum performed onto the composite indicating any significant change in the characteristic FTIR peak of the TOCgel (C–O–C ether bonds at 1030 cm^{-1}) which is clearly similar to those of the pure TOCgel (Figure 5). Thus, the TOCgel backbone was maintained after the hydrothermal synthesis, suggesting that there was some degradation of the TOCgel.

Moreover, the FTIR spectrum of TOCgel exhibits a peak at 1610 cm^{-1} corresponding to the carboxylate groups. The position of this peak appears to be slightly shifted in the former composite film ($\sim 1625\text{ cm}^{-1}$), which could be related to the adsorption of carboxylate onto ZnO structures [41,55].

To further prove the presence of ZnO superstructures incorporated in the TOCgel/ZnO composite film, X-ray photoelectron spectroscopic study has been used. As can be seen in XPS spectra (Figure 6A), XPS survey spectra of the composite shows three main peaks, one peak at 532 eV corresponding to O 1s, one peak at 285 eV corresponding to C 1s, and two peaks at 1020–1045 eV corresponding to Zn 2p. Of course, the presence of Zn element is due to ZnO structures present in the final composite.

Moreover, high resolution scans of the XPS spectra of Zn 2p (Figure 6B) can be decomposed into two main components centered at 1020.2 and 1045.3 eV which correspond to Zn 2p_{3/2} and Zn 2p_{1/2}, respectively. According to the literature, these subpeaks of the Zn 2p were found to be related to Zn–O bonding in ZnO [56]. In addition, the peak corresponding to the nitrogen element appears to be very weak (0.17%) which is possibly due to the fact that the obtained composite film may be possibly free of residual HMT and nitrate ions. In addition, the increase in O/C ratio from 0.58 to 0.97 for the TOCgel/ZnO composite can be attributed to the incorporation of ZnO structures (rich in oxygen atoms)

within the fibrous structure of the cellulose. We also observed that the O/C ratio (0.58) is similar to that of the pure TOCgel [57], which confirms that the TOCgel structure did not significantly alter during the hydrothermal synthesis.

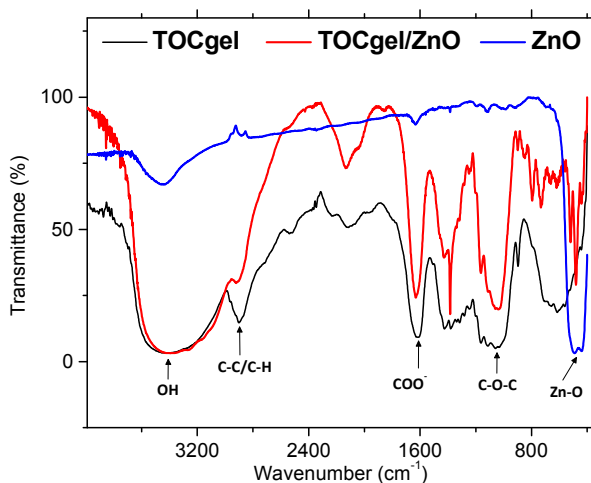


Figure 5. FTIR spectra of TOCgel/ZnO composite, pure TOCgel, and pure ZnO.

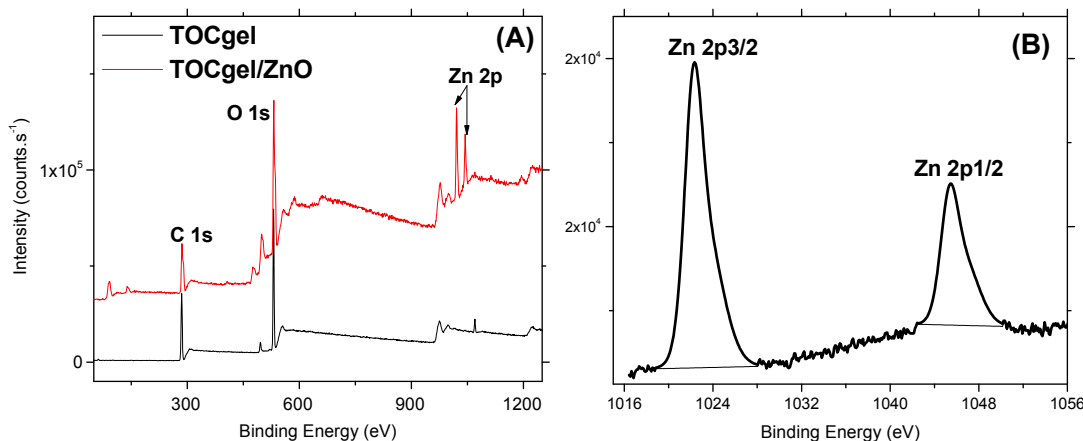
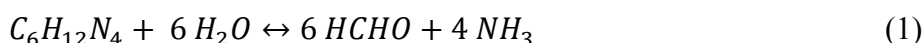
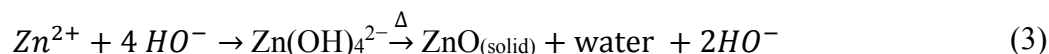


Figure 6. XPS survey spectra of the TOCgel/ZnO composite and the pure TOCgel (A); and high-resolution XPS scan of Zn 2p in the TOCgel/ZnO composite (B).

3.4. Mechanism of the Formation of Flower-Like ZnO Superstructures

The synthesis of ZnO flower-like structures was performed directly onto TOCgel surfaces through hydrothermal routes with some modification from the previous literature [34,41]. Indeed, the growth of ZnO superstructures onto the TOCgel surface can be related to the treatment of TOCgel with both Zinc nitrate and HMT solutions, which led to the nucleation and the growth of discrete seeds at the cellulosic fiber surface. Herein, HMT was used as a pH buffer by a slow release of OH⁻ ions in the reaction medium to facilitate the controlled growth of ZnO particles through thermal decomposition as follows [58]:





As mentioned in Equations (1)–(3), HMT releases slowly hydroxide ions in the medium, and then, zinc cations bound to OH^- through coordination or electrostatic interaction, forming the complex $\text{Zn}(\text{OH})_4^{2-}$ which contribute to the formation of ZnO nucleated via thermal treatment of the solution of $\text{Zn}(\text{OH})_4^{2-}$ onto the TOCgel surface. In this study, the presence of polar moieties (COO^- and OH) at the surface of TOCgel fibers should be responsible for the improvement of the heterogeneous nucleation of ZnO particles. The origin of this improvement lies especially in electrostatic forces that occur between COO^- moieties of TOCgel and Zn^{2+} ions introduced in the reaction medium. With the reaction proceeding, ZnO nanoparticles formed onto TOCgel surfaces would be aggregated into larger structures in order to minimize the total surface energy, which results in the formation of numerous spherical ZnO aggregations in the medium due to the Ostwald ripening [59]. Moreover, the very high concentration of carboxylate anions presented in the reaction medium could be responsible for the formation of such ZnO nanosheets. Indeed, with the reaction proceeding, the initial fast nucleation of ZnO leads to the decrease of the concentration of ZnO_2^{2-} monomer. Thus, the adsorption of COO^- ions on the positively charged Zn-(0001) plane would dominate in the competition with ZnO_2^{2-} growth units. According to the literature [34,60–62], the excess of COO^- species stabilizes the surface charge and the structure of Zn-(0001) surfaces to some extent, retard growth along the *c*-axis and promotes the fast growth along the *a*-axis (0110) which results in the formation of ZnO nanosheets with a {2110} planar surface as illustrated in Figure 7.

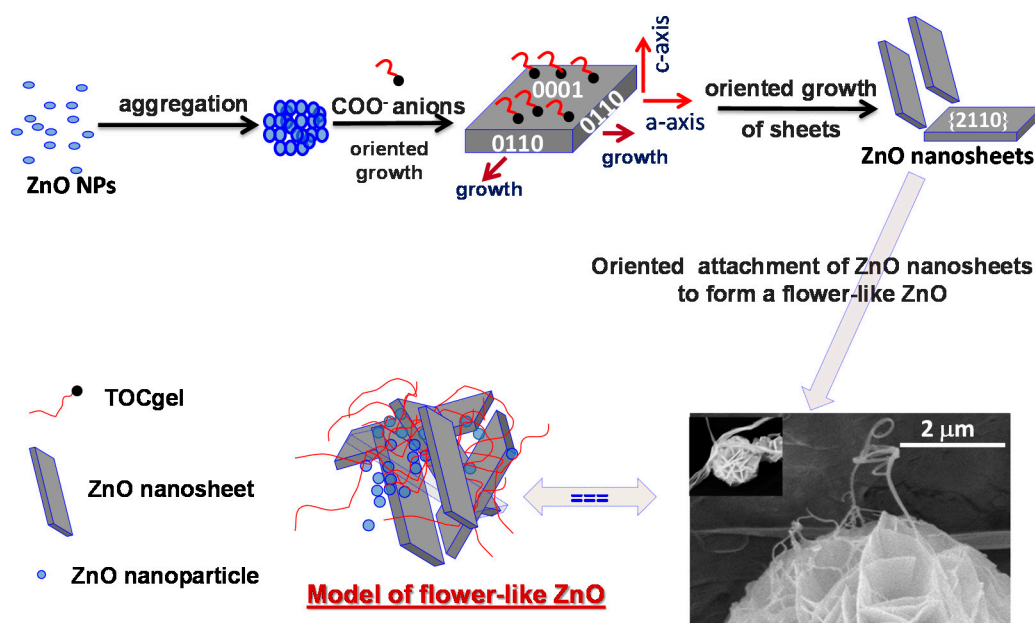


Figure 7. Schematic illustration of the proposed mechanism explaining the formation of flower-like ZnO superstructures.

After that, these primary ZnO nanosheets (average thickness of ~ 80 nm) might have many crystalline boundaries on their surfaces, which displayed more defects than other regions and were thermodynamically unstable. Consequently, they would tend to further diminish their energy through surface reconstruction, which would provide active sites for secondary heterogeneous nucleation and growth according to the literature [34,63].

In this context, the presence of these active sites would promote the adsorption of carboxylate moieties of TOCgel (as a surfactant) especially onto the reactive planes of ZnO, usually the (001) plane [64], which would affect the secondary nucleation. Consequently, such adsorption could facilitate the secondary structure nucleation on the initial structure (through the intersection of nanosheets) in order to reduce the interfacial activation energy, and finally contribute to the construction of the well-shaped flower-like ZnO superstructures with porous surfaces within the former TOCgel/ZnO composite film as illustrated in Figure 7. Earlier, several researchers have also demonstrated the effect of citrate and ascorbate solutions on the formation of flower-like ZnO structures under hydrothermal route [34,41]. In our work, carboxylate moieties present along the oxidized cellulose fibers display similar effects in the tuning of the shape of ZnO and, fortunately contribute to the elaboration of a flexible composite material in which flower-ZnO superstructures are well-dispersed within the fibrous network of TOCgel as confirmed by the SEM images (Figure 2).

3.5. Thermal Stability

Figure 8 showed the thermogravimetric curves of pure ZnO, pure TOCgel and TOCgel/ZnO composite which were recorded under inert atmosphere. Both materials contain a few layers of moisture, which were eliminated at 105 °C. As can be seen in the thermogram curve, the decomposition of the pure TOCgel between 250 and 300 °C was attributed to the destruction of the crystalline region of the cellulose fiber and decomposition of amorphous region into a monomer of D-glucopyranose and followed by the major thermal-oxidative degradation of the organic part from 580 °C [57,65].

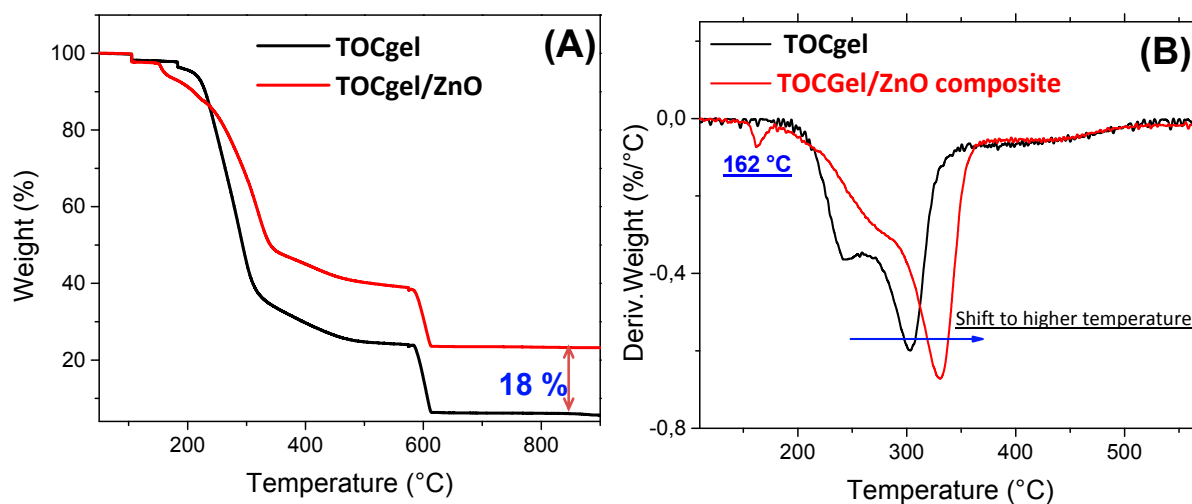


Figure 8. Representative TGA curves (A) and DTGA curves (B) of pure TOCgel and TOCgel/ZnO composite.

In comparison with the TOCgel/ZnO composite film, TG curves demonstrated clearly that the latter exhibits higher thermal stability than pure TOCgel, which can be clearly highlighted by the ability of ZnO superstructures well-dispersed within the fibrous network to protect TOCgel nanofibers. Several works indicated that the thermal stability of carbohydrate (*i.e.*, starch, cellulose) did not change after incorporation of ZnO [66,67].

However, our result demonstrated the thermal stability enhanced with TOCgel after the incorporation of ZnO flower-like superstructures. This contradiction could be explained by the strong interaction electrostatic/hydrogen bonding between the carboxylate moieties of TOCgel and ZnO flower-like superstructures, which contributes to the shift observed in the thermal degradation temperature of TOCgel from 300 to 335 °C which, in turn, offer thermal processing advantages. We also observed a low transition (at 162 °C) in the DTG curve of the final composite film. According to the literature, this transition can be assigned to the loss of water trapped in the composite film and the decomposition of some incorporated HMT or nitrate ions possibly remained in the composite [66]. Moreover, after combustion of all organic parts in the TOCgel/ZnO composite (under air atmosphere), the residual amount (~18% by weight) corresponds to ZnO as shown in Figure 8.

3.6. Mechanical Properties

In order to investigate the mechanical behavior of the TOCgel/ZnO composite film, tensile tests were performed on the both samples (TOCgel, composite and ZnO). As shown in Figure 9A, the tensile curve of pure ZnO is not shown due to the poor mechanical properties of ZnO powders and the high brittleness of the ZnO film.

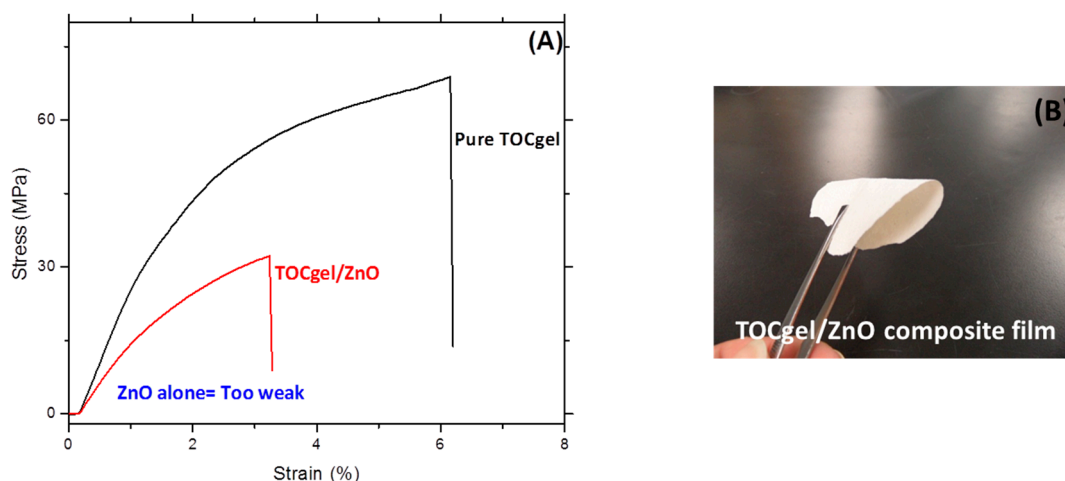


Figure 9. Tensile stress-strain behaviors of pure TOCgel and the TOCgel/ZnO composite films (A); and optical image of the composite film (B).

Indeed, Interfacial interaction between ZnO and TOCgel appears to be an important factor affecting the mechanical properties of the composite film. In our work, results showed that the incorporation of ZnO within the fibrous network of the TOCgel enhances the mechanical behavior of the composite film through the well-dispersed state and strongest interactions of ZnO onto cellulose fibers surfaces. Of course, the mechanical behavior of the composite remained lower comparatively to that of the pure

TOCgel. However, the composite film maintains some flexibility (bending up to 120°) as shown in the optical image (Figure 9B). In conclusion, by making a coating of ZnO flower-like superstructures onto the flexible TOCgel matrix, flexibility can be introduced without loss of its photocatalytic properties.

3.7. Photocatalytic Degradation

The photocatalytic activity of pure ZnO (rod-like), TOCgel/ZnO (FL) and native cellulose/ZnO (aggregated nanoparticles) in the degradation of MB was performed in air at room temperature and under the exposure of the ultraviolet lamp for 2 h. The MB was chosen in this work due to their strong adsorption characteristics on many surfaces, good resistance to light degradation and a well, defined optical absorption band in the visible region [67].

From Figure 10A, it can be observed that the absorption peak intensity of MB in the 500–700 nm regions (especially at 665 nm) decreases rapidly, compared to the intensity of the initial MB solution, because supported ZnO structures promotes the catalytic photodegradation [68]. This result was also confirmed by the significant change in the coloration of dried samples (from blue to violet) under the exposure to the UV light lamp for about two hours as represented in the optical images (Figure 10B). The violet color of irradiated sample could be related to the degradation state of MB molecules through the photocatalysis effect of flower-like ZnO superstructures embedded in the TOCgel/ZnO composite material. Of course, the coloration change and the decrease of the absorption peak of MB were more pronounced in the case of the pure ZnO, because this sample consist in a 100% ZnO particles. However, in the case of composites, the amount of ZnO was about 15%–20% (*w/w*) as determined by the thermal analysis (Figure 9).

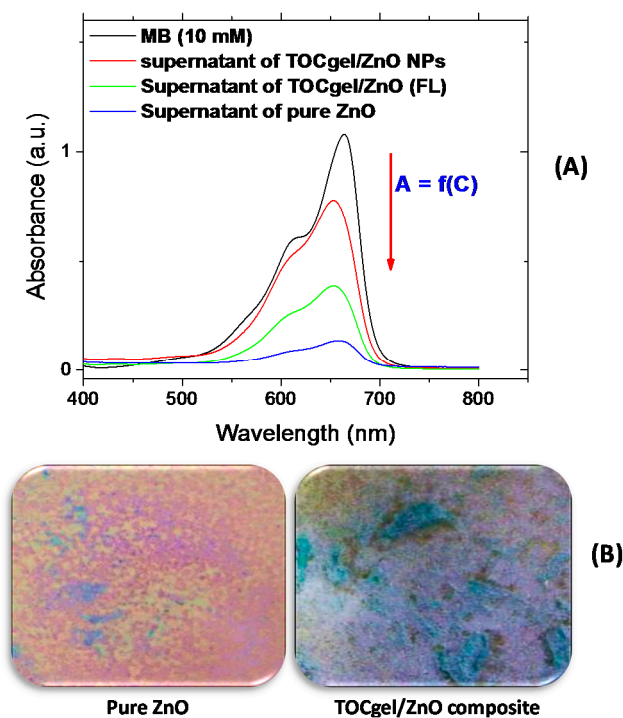


Figure 10. UV-Vis spectra of different supernatants of MB obtained after UV-irradiation for 2 h; (A) optical images of corresponding dried samples after photocatalytic process for pure ZnO and TOCgel materials (B).

According to the literature [69], the photocatalytic process of ZnO can be elucidated by the photogeneration process as illustrated in the Figure 11.

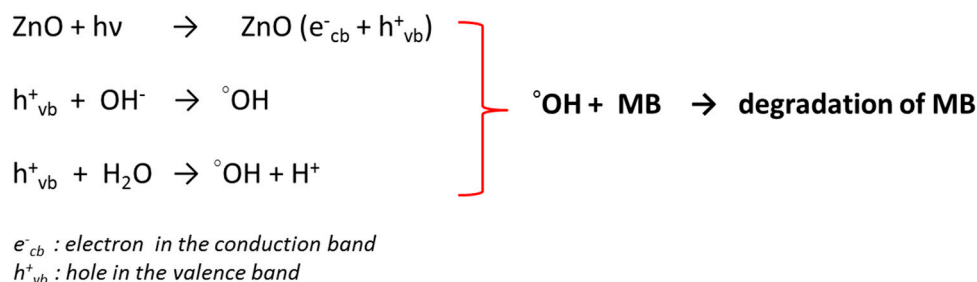


Figure 11. Schematic representation of the photocatalytic process of the ZnO in the degradation of the MB.

In fact, the UV radiation absorbed by ZnO induces the formation of electron-hole pairs through the photogeneration process. Then, the interaction between holes and hydroxyl groups of ZnO contributes to the formation of the strong oxidative hydroxyl radicals (${}^\circ\text{OH}$). Furthermore, H_2O could also react with holes to form hydroxyl radicals. Thus, the strong oxidant property of the hydroxyl radical lead to the oxidation of organic materials, and of course to the degradation of MB as shown in Figure 10.

In the present study, it appears interesting to appoint the effect of the morphology of ZnO structures onto their photocatalytic degradation efficiency in the degradation of MB solution.

To further explain this, a further experiment was performed using other morphologies of ZnO under the same conditions to demonstrate the effect of ZnO morphologies on the photocatalytic efficiency of ZnO structures. In this context, we investigated the photocatalytic performance of native cellulose/ZnO composite in the degradation of MB solution under the UV irradiation for 2 h. As shown in Figure 10A, the decrease of the absorption peak (at 665 nm) appears to be more pronounced in the case of TOCgel/ZnO (FL) than that of native cellulose/ZnO (aggregated nanoparticles), which clearly indicates the influence of ZnO morphologies on the photocatalytic degradation process. Our results are in clear accordance with the literature in which flower-like ZnO structures exhibit the highest catalytic activity efficiency more than other structures such as spindlelike, swordlike, commercial ZnO materials [13,52]. As shown in the SEM images (Figure 3); we demonstrated that the oxidized cellulose or TOCgel (rich in carboxylate groups) should be responsible for the formation of flower-like ZnO superstructures in the former composite, which was not the case of the oxidized cellulose.

4. Conclusions

In this paper, we report a simple and efficient hydrothermal method of preparing mainly flower-like ZnO superstructures with controllable sizes using TEMPO-oxidized nanocellulose gel (TOCgel) as a shape-directing/capping agent in the presence of an amine at ambient temperature.

The former composite film based on the TOCgel and ZnO superstructures exhibited high flexibility (bent up to 120°) and characterized by good thermal and photocatalytic properties. FTIR and XPS data confirmed the presence of Zn–O bond of ZnO structures in the former composite. We also demonstrated the contribution of carboxylate groups of TOCgel in the tuning of the shape and size of zinc oxide

superstructures, which were well-dispersed within the fibrous structure of the cellulosic material. In fact, carboxylate groups of TOCgel act as capping agents during the hydrothermal synthesis, which adsorb to a particular crystal facet (polar plane-001) and enhance the secondary structure nucleation on the initial structure (through the intersection of nanosheets) in order to reduce the total energy of the system, and contribute to the construction of the well-shaped flower-like ZnO superstructures with porous surfaces into the former composite.

Finally, because of the high flexibility, good mechanical, thermal and photocatalytic properties of the former TOCgel/ZnO composite films, they can be suitable in applications of disposable electronic devices, sensors, piezo-electric devices, photo-catalytic systems, and actuations.

Acknowledgments

The authors gratefully acknowledge the Natural Science and Engineering Research Council of Canada (NSERC) for financial support.

Author Contributions

Khalil Jradi and Chloé Maury conceived and designed the experiments; Chloé Maury performed the experiments; Khalil Jradi analyzed the data and wrote the paper; Claude Daneault contributed reagents/materials/analysis tools; Claude Daneault Supervising the project and revision of the manuscript.

Conflicts of Interest

The authors declare no conflict of interest.

References

1. Wiley, B.; Sun, Y.; Xia, Y. Synthesis of silver nanostructures with controlled shapes and properties. *Acc. Chem. Res.* **2007**, *40*, 1067–1076.
2. Xiong, Y.; Xia, Y. Shape-Controlled Synthesis of Metal Nanostructures: The Case of Palladium. *Adv. Mater.* **2007**, *19*, 3385–3391.
3. Sun, Y.G.; Xia, Y.N. Shape-Controlled Synthesis of Gold and Silver Nanoparticles. *Science* **2002**, *298*, 2176–2179.
4. Wen, F.; Zhang, W.Q.; Wei, G.W.; Wang, Y.; Zhang, J.Z.; Zhang, M.C.; Shi, L.Q. Synthesis of Noble Metal Nanoparticles Embedded in the Shell Layer of Core–Shell Poly(styrene-co-4-vinylpyridine) Microspheres and Their Application in Catalysis. *Chem. Mater.* **2008**, *20*, 2144–2150.
5. Hu, Y.F.; Zhang, Y.; Chang, Y.L.; Snyder, R.L.; Wang, Z.L. Optimizing the Power Output of a ZnO Photocell by Piezopotential. *ACS Nano* **2010**, *4*, 4220–4224.
6. Wang, Z.L.; Song, J.H. Piezoelectric Nanogenerators Based on Zinc Oxide Nanowire Arrays. *Science* **2006**, *312*, 242–246.
7. Ye, C.; Bando, Y.; Shen, G.; Golberg, D.J. Thickness-Dependent Photocatalytic Performance of ZnO Nanoplatelets. *Phys. Chem. B* **2006**, *110*, 15146–15151.
8. Liu, B.; Zeng, H.C. Room Temperature Solution Synthesis of Monodispersed Single-Crystalline ZnO Nanorods and Derived Hierarchical Nanostructures. *Langmuir* **2004**, *20*, 4196–4204.

9. Zhang, H.; Yang, D.; Ma, X.Y.; Que, D. Synthesis and Field Emission Characteristics of Bilayered ZnO Nanorod Array Prepared by Chemical Reaction. *J. Phys. Chem. B* **2005**, *109*, 17055–17059.
10. Wang, X.D.; Summers, C.J.; Wang, Z.L. Large-Scale Hexagonal-Patterned Growth of Aligned ZnO Nanorods for Nano-optoelectronics and Nanosensor Arrays. *Nano Lett.* **2004**, *4*, 423–426.
11. Campbell, J.L.; Breedon, M.; Latham, K.; Kalantar-zadeh, K. Electrowetting of Superhydrophobic ZnO Nanorods. *Langmuir* **2008**, *24*, 5091–5098.
12. Laurenti, M.; Verna, A.; Chiolerio, A. Evidence of negative capacitance in piezoelectric ZnO thin films sputtered on interdigital electrodes. *ACS Appl. Mater. Interfaces* **2015**, doi:10.1021/acsami.5b05336.
13. Han, X.G.; He, H.Z.; Kuang, Q.; Zhou, X.; Zhang, X.H.; Xu, T. Controlling Morphologies and Tuning the Related Properties of Nano/Microstructured ZnO Crystallites. *J. Phys. Chem. C* **2009**, *113*, 584–589.
14. Lao, J.Y.; Wen, I.G.; Ren, Z.F. Hierarchical ZnO Nanostructures. *Nano Lett.* **2002**, *2*, 1287–1291.
15. Cho, S.G.; Jang, J.W.; Lee, J.S.; Lee, K.H. Exposed Crystal Face Controlled Synthesis of 3D ZnO Superstructures. *Langmuir* **2010**, *26*, 14255–14262.
16. Xiang, B.; Wang, P.; Zhang, X.; Dayeh, S.A.; Aplin, D.P.R.; Soci, C.; Yu, D.; Wang, D. Rational Synthesis of *p*-Type Zinc Oxide Nanowire Arrays Using Simple Chemical Vapor Deposition. *Nano Lett.* **2007**, *7*, 323–328.
17. Wang, F.; Cao, L.; Pan, A.; Liu, R.; Wang, X.; Zhu, X.; Wang, S.; Zou, B. Synthesis of Tower-like ZnO Structures and Visible Photoluminescence Origins of Varied-Shaped ZnO Nanostructures. *J. Phys. Chem. C* **2007**, *111*, 7655–7660.
18. Gu, Z.; Paranthaman, M.P.; Xu, J.; Pan, Z. Aligned ZnO Nanorod Arrays Grown Directly on Zinc Foils and Zinc Spheres by a Low-Temperature Oxidization Method. *ACS Nano* **2009**, *3*, 273–278.
19. Yano, S.; Maeda, H.; Nakajima, M.; Hagiwara, T.; Sawaguchi, T. Preparation and mechanical properties of bacterial cellulose nanocomposites loaded with silica nanoparticles. *Cellulose* **2008**, *15*, 111–120.
20. Maneerung, T.; Tokura, S.; Rujiravanit, R. Impregnation of silver nanoparticles into bacterial cellulose for antimicrobial wound dressing. *Carbohydr. Polym.* **2008**, *72*, 43–51.
21. Chiolerio, A.; Roppolo, I.; Cauda, V.; Crepaldi, M.; Bocchini, S.; Bejtka, K.; Verna, A.; Pirri, C.F. Ultraviolet mem-sensors: Flexible anisotropic composites featuring giant photocurrent enhancement. *Nano Res.* **2015**, *8*, 1956–1963.
22. Tian, Z.R.; Voigt, J.A.; Liu, J.; Mckenzie, B.; Mcdermott, M.J.J. Biomimetic arrays of oriented helical ZnO nanorods and columns. *Am. Chem. Soc.* **2002**, *124*, 12954–12955.
23. Sounart, T.L.; Liu, J.; Voigt, J.A.; Huo, M.; Spoerke, E.D.; Mckenzie, B. Secondary nucleation and growth of ZnO. *J. Am. Chem. Soc.* **2007**, *129*, 15786–15793.
24. Muoz-Espi, R.; Jeschke, G.; Lieberwirth, I.; Gmez, C.M.; Wegner, G.J. ZnO–Latex Hybrids Obtained by Polymer-Controlled Crystallization: A Spectroscopic Investigation. *Phys. Chem. B* **2007**, *111*, 697–707.
25. Zhang, H.; Yang, D.; Li, D.; Ma, X.; Li, S.; Que, D. Controllable Growth of ZnO Microcrystals by a Capping-Molecule-Assisted Hydrothermal Process. *Cryst. Growth Des.* **2005**, *5*, 547–550.

26. Rashid, M.H.; Raula, M.; Bhattacharjee, R.R.; Mandal T.K. Low-temperature polymer-assisted synthesis of shape-tunable zinc oxide nanostructures dispersible in both aqueous and non-aqueous media. *Colloid Interface Sci.* **2009**, *339*, 249–258.
27. Tian, Z.R.; Voigt, J.A.; Liu, J.; McKenzie, B.; McDermott, M.J.; Rodriguez, M.A.; Konishi, H.; Xu, H. Complex and oriented ZnO nanostructures. *Nat. Mater.* **2003**, *2*, 821–826.
28. Cho, S.; Jang, J.; Jung, S.; Lee, B.R.; Oh, E.; Lee, K. Precursor Effects of Citric Acid and Citrates on ZnO Crystal Formation. *Langmuir* **2009**, *25*, 3825–3831.
29. Du, J.; Liu, Z.; Huang, Y.; Gao, Y.; Han, B.; Li, W.; Yang, G.J. Control of ZnO morphologies via surfactants assisted route in the subcritical water. *Cryst. Growth.* **2005**, *280*, 126–134.
30. Guo, L.; Ji, Y.L.; Xu, H.; Simon, P.; Wu, Z.J. Regularly Shaped, Single-Crystalline ZnO Nanorods with Wurtzite Structure. *Am. Chem. Soc.* **2002**, *124*, 14864–14865.
31. Zhang, X.L.; Qiao, R.; Qiu, R.; Kim, J.C.; Kang, Y.S. Fabrication of Hierarchical ZnO Nanostructures via a Surfactant-Directed Process. *Cryst. Growth Des.* **2009**, *9*, 2906–2910.
32. Pal, U.; Santiago, P.J. Controlling the Morphology of ZnO Nanostructures in a Low-Temperature Hydrothermal Process. *Phys. Chem. B* **2005**, *109*, 15317–15321.
33. Umetsu, M.; Mizuta, M.; Tsumoto, K.; Ohara, S.; Takami, S.; Watanabe, H.; Kumagai, I.; Adschiri, T. Bioassisted Room-Temperature Immobilization and Mineralization of Zinc Oxide—The Structural Ordering of ZnO Nanoparticles into a Flower-Type Morphology. *Adv. Mater.* **2005**, *17*, 2571–2575.
34. Sun, Y.; Wang, L.; Yu, X.; Chen, K. Facile synthesis of flower-like 3D ZnO superstructures via solution route. *Cryst. Eng. Comm.* **2012**, *14*, 3199–3204.
35. Li, J.; Fan, H.Q.; Jia, X.H. Multilayered ZnO Nanosheets with 3D Porous Architectures: Synthesis and Gas Sensing Application. *J. Phys. Chem. C* **2010**, *114*, 14684–14691.
36. Gazia, R.; Chiodoni, A.; Bianco, S.; Lamberti, A.; Quaglio, M.; Sacco, A.; Tresso, E.; Mandracci, P.; Pirri, C.F. An easy method for the room-temperature growth of spongelike nanostructured Zn films as initial step for the fabrication of nanostructured ZnO. *Thin Solid Films* **2012**, *524*, 107–112.
37. Ko, S.H.; Lee, D.; Kang, H.W.; Nam, K.H.; Yeo, J.Y.; Hong, S.J.; Sung, H.J. Nanoforest of Hydrothermally Grown Hierarchical ZnO Nanowires for a High Efficiency Dye-Sensitized Solar Cell. *Nano Lett.* **2011**, *11*, 666–671.
38. Lu, F.; Cai, W.P.; Zhang, Y.G. ZnO hierarchical micro/nanoarchitectures: Solvothermal synthesis and structurally enhanced photocatalytic performance. *Adv. Funct. Mater.* **2008**, *18*, 1047–1056.
39. Wu, Q.; Chen, X.; Zhang, P.; Han, Y.; Chen, X.; Yan, Y.; Li, S. Amino Acid-Assisted Synthesis of ZnO Hierarchical Architectures and Their Novel Photocatalytic Activities. *Cryst. Growth Des.* **2008**, *8*, 3010–3018.
40. Yin, J.; Lu, Q.; Yu, Z.; Wang, J.; Pang, H.; Gao, F. Hierarchical ZnO Nanorod-Assembled Hollow Superstructures for Catalytic and Photoluminescence Applications. *Cryst. Growth Des.* **2010**, *10*, 40–43.
41. Raula, M.; Harunar Rashid, M.; Paira, T.K.; Dinda, E.; Mandal, T.K. Ascorbate-Assisted Growth of Hierarchical ZnO Nanostructures: Sphere, Spindle, and Flower and Their Catalytic Properties. *Langmuir* **2010**, *26*, 8769–8782.
42. Thomas, V.; Namdeo, M.; Mohan, Y.M.; Bajpai, S.K.; Bajpai, M. Review on polymer, hydrogel and microgel metal nanocomposites: A facile nanotechnological approach. *J. Macromol. Sci. A* **2008**, *45*, 107–119.

43. Yang, K.K.; Wang, X.L.; Wang, Y.Z. Progress in Nanocomposite of Biodegradable Polymer. *J. Ind. Eng. Chem.* **2007**, *13*, 485–500.
44. Kim, J.; Yun, S.; Ounaies, Z. Discovery of cellulose as a smart material. *Macromolecules* **2006**, *39*, 4202–4206.
45. John, A.; Ko, H.U.; Kim, D.G.; Kim, J. Preparation of cellulose-ZnO hybrid films by a wet chemical method and their characterization. *Cellulose* **2011**, *18*, 675–680.
46. Goncalves, G.; Marques, P.A.A.P.; Neto, C.P.; Trindade, T.; Peres, M.; Monteiro, T. Growth, structural, and optical characterization of ZnO-coated cellulosic fibers. *Cryst. Growth Des.* **2009**, *9*, 386–390.
47. Loranger, E.; Piché, A.O.; Daneault, C. Influence of High Shear Dispersion on the Production of Cellulose Nanofibers by Ultrasound-Assisted TEMPO-Oxidation of Kraft Pulp. *Nanomaterials* **2012**, *2*, 286–297.
48. Mishra, S.P.; Thirree, J.; Manent, A.S.; Chabot, B.; Daneault, C. Ultrasound-catalyzed TEMPO-mediated oxidation of native cellulose for the production of nanocellulose: Effect of process variables. *BioResources* **2011**, *6*, 121–143.
49. Saito, T.; Nishiyama, Y.; Putaux, J.L.; Vignon, M.; Isogai, A. Homogeneous suspensions of individualized microfibrils from TEMPO-catalyzed oxidation of native cellulose. *Biomacromolecules* **2006**, *7*, 1687–1691.
50. Loranger, E.; Paquin, M.; Daneault, C.; Chabot, B. Comparative study of sonochemical effects in an ultrasonic bath and in a large-scale flow-through sonoreactor. *Chem. Eng. J.* **2011**, *178*, 359–365.
51. Okita, Y.; Saito, T.; Isogai, A. Entire surface oxidation of various cellulose microfibrils by TEMPO-mediated oxidation. *Biomacromolecules* **2010**, *11*, 1696–1700.
52. Wang, X.; Zhang, Q.; Wan, Q.; Dai, G.; Zhou, C.; Zou, B. Controllable ZnO Architectures by Ethanolamine-Assisted Hydrothermal Reaction for Enhanced Photocatalytic Activity. *J. Phys. Chem. C* **2011**, *115*, 2769–2775.
53. Sugunan, A.; Warad, H.C.; Boman, M.; Dutta, J. Zinc oxide nanowires in chemical bath on seeded substrates: Role of hexamine. *J. Sol Gel Sci. Technol.* **2006**, *39*, 49–56.
54. Bhadra, P.; Mitra, M.K.; Das, G.C.; Dey, R.; Mukherjee, S. Interaction of chitosan capped ZnO nanorods with Escherichia coli. *Mater. Sci. Eng. C* **2011**, *31*, 929–937.
55. Dinda, E.; Si, S.; Kotal, A.; Mandal, T.K. Novel Ascorbic Acid Based Ionic Liquids for the *in Situ* Synthesis of Quasi-Spherical and Anisotropic Gold Nanostructures in Aqueous Medium. *Chem. Eur. J.* **2008**, *14*, 5528–5537.
56. Pan, K.Y.; Lin, Y.H.; Lee, P.S.; Wu, J.M.; Shih, H.C. Synthesis of SnO₂-ZnO Core-Shell Nanowires and Their Optoelectronic Properties. *J. Nanomater.* **2012**, doi:10.1155/2012/279245.
57. Benkaddour, A.; Journoux-Lapp, C.; Jradi, K.; Robert, S.; Daneault, C. Study of the hydrophobization of TEMPO-oxidized cellulose gel through two routes: Amidation and esterification process. *J. Mater. Sci.* **2014**, *49*, 2832–2843.
58. Govender, K.; Boyle, D.S.; Kenway, P.B.; O'Brien, P. Understanding the factors that govern the deposition and morphology of thin films of ZnO from aqueous solution. *J. Mater. Chem.* **2004**, *14*, 2575–2591.
59. Li, Q.Y.; Wang, E.B.; Li, S.H.; Wang, C.L.; Tian, C.G. Template-free polyoxometalate-assisted synthesis for ZnO hollow spheres. *J. Solid State Chem.* **2009**, *182*, 1149–1155.

60. Pacholski, C.; Kornowski, A.; Weller, H. Self-Assembly of ZnO: From Nanodots to Nanorods. *Angew. Chem. Int. Ed.* **2002**, *41*, 1188–1191.
61. Zhang, D.F.; Sun, L.D.; Yin, J.L.; Yan, C.H.; Wang, R.M. Attachment-Driven Morphology Evolution of Rectangular ZnO Nanowires. *J. Phys. Chem. B* **2005**, *109*, 8786–8790.
62. Li, B.; Wang, Y. Facile synthesis and enhanced photocatalytic performance of Flower-like ZnO hierarchical microstructures. *J. Phys. Chem. C* **2010**, *114*, 890–896.
63. Gao, Y.F.; Koumoto, K. Bioinspired Ceramic Thin Film Processing: Present Status and Future Perspectives. *Cryst. Growth Des.* **2005**, *5*, 1983–2017.
64. Yang, H.G.; Sun, C.H.; Qiao, S.Z.; Zou, J.; Liu, G.; Smith, S.C.; Cheng, H.M.; Lu, G.Q. Anatase TiO₂ single crystals with a large percentage of reactive facets. *Nature* **2008**, *453*, 638–641.
65. Rambo, C.R.; Recouvreux, D.O.S.; Carminatti, C.A.; Pitlovanciv, A.K.; Antonio, R.V.; Porto, L.M. Template assisted synthesis of porous nanofibrous cellulose membranes for tissue engineering. *Mater. Sci. Eng. C* **2008**, *28*, 549.
66. Mumalo-Djokic, D.; Stern, W.B.; Taubert, A. Zinc Oxide/Carbohydrate Hybrid Materials via Mineralization of Starch and Cellulose in the Strongly Hydrated Ionic Liquid Tetrabutylammonium Hydroxide. *Cryst. Growth Des.* **2008**, *8*, 330–335.
67. Moafi, H.F.; Shojaie, A.F.; Zanjanchi, M.A. Photocatalytic self-cleaning properties of cellulosic fibers modified by nano-sized zinc oxide. *Thin Solid Films* **2011**, *519*, 3641–3646.
68. Chakrabarti, S.; Dutta, B.K. Photocatalytic degradation of model textile dyes in wastewater using ZnO as semiconductor catalyst. *J. Hazard. Mater.* **2004**, *112*, 269–278.
69. Yatmaz, H.C.; Akyol, A.; Bayramoglu, M. Kinetics of the Photocatalytic Decolorization of an Azo Reactive Dye in Aqueous ZnO Suspensions. *Ind. Eng. Chem. Res.* **2004**, *43*, 6035–6039.

© 2015 by the authors; licensee MDPI, Basel, Switzerland. This article is an open access article distributed under the terms and conditions of the Creative Commons Attribution license (<http://creativecommons.org/licenses/by/4.0/>).